A common dimerization interface in bacterial response regulators KdpE and TorR

ALEJANDRO TORO-ROMAN,[1,2] TI WU,[2,3] AND ANN M. STOCK[2,3,4]

[1]Department of Chemistry and Chemical Biology, Rutgers University, Piscataway, New Jersey 08854, USA
[2]Center for Advanced Biotechnology and Medicine and [3]Howard Hughes Medical Institute, Piscataway, New Jersey 08854, USA
[4]Department of Biochemistry, University of Medicine and Dentistry of New Jersey, Robert Wood Johnson Medical School, Piscataway, New Jersey 08854, USA

(RECEIVED July 23, 2005; FINAL REVISION September 1, 2005; ACCEPTED September 1, 2005)

Abstract

Bacterial response regulators are key regulatory proteins that function as the final elements of so-called two-component signaling systems. The activities of response regulators in vivo are modulated by phosphorylation that results from interactions between the response regulator and its cognate histidine protein kinase. The level of response regulator phosphorylation, which is regulated by intra- or extracellular signals sensed by the histidine protein kinase, ultimately determines the output response that is initiated or carried out by the response regulator. We have recently hypothesized that in the OmpR/PhoB subfamily of response regulator transcription factors, this activation involves a common mechanism of dimerization using a set of highly conserved residues in the α4–β5–α5 face. Here we report the X-ray crystal structures of the regulatory domains of response regulators TorR (1.8 Å), Ca^{2+}-bound KdpE (2.0 Å), and Mg^{2+}/BeF_3^--bound KdpE (2.2 Å), both members of the OmpR/PhoB subfamily from *Escherichia coli*. Both regulatory domains form symmetric dimers in the asymmetric unit that involve the α4–β5–α5 face. As observed previously in other OmpR/PhoB response regulators, the dimer interfaces are mediated by highly conserved residues within this subfamily. These results provide further evidence that most all response regulators of the OmpR/PhoB subfamily share a common mechanism of activation by dimerization.

Keywords: phosphorylation; transcription regulation; response regulator; TMAO respiratory system; Kdp K^+ transport system

Two-component systems (TCSs) that function as phosphotransfer pathways are among the most commonly used signaling mechanisms in bacteria. These TCSs allow bacteria to respond to and survive changes in their environments by regulating a variety of cellular activities/events such as chemotaxis, quorum sensing, and stress responses (Lukat and Stock 1993; Kleerebezem et al. 1997; Raivio and Silhavy 1997). A TCS in its simplest form consists of a histidine protein kinase and a response regulator (RR) protein, but systems can be further expanded to involve multiple phosphorelay reactions. RRs, which contain a conserved regulatory domain capable of accepting a phosphoryl group at an active site aspartate, serve as phosphorylation-dependent molecular "switches" and are generally found at the ends of these signaling pathways. The lifetime of phosphorylated RRs ranges from seconds to hours, a function of the autophosphatase activity of RRs and the

Reprint requests to: Ann M. Stock, Center for Advanced Biotechnology and Medicine, 679 Hoes Lane, Piscataway, NJ 08854, USA; e-mail: stock@cabm.rutgers.edu; fax: (732) 235-5289.

Abbreviations: TCS(s), two-component system(s); RR(s), response regulator(s); $KdpE_N$, KdpE regulatory domain; $TorR_N$, TorR regulatory domain; NCS, noncrystallographic symmetry; RMSD, root mean square deviation; TMAO, trimethylamine *N*-oxide; SeMet, selenomethionine; βME, β-mercaptoethanol; PDB, Protein Data Bank.

Article and publication are at http://www.proteinscience.org/cgi/doi/10.1110/ps.051722805.

inherent instability of the acyl phosphate modification. Beryllofluoride (BeF_3^-), a noncovalent complex that mimics the phosphoryl group (Chabre 1990; Yan et al. 1999; Cho et al. 2001), has been used extensively to lock RRs in their active states for structural and biochemical analyses.

Multiple-domain RRs can be classified by their effector domain architecture with the major group consisting of transcription factors (for reviews, see Robinson et al. 2000 and Stock et al. 2000). The largest subclass of RR transcription factors is the OmpR/PhoB subfamily, which, in *Escherichia coli*, accounts for almost half of the RRs in the genome (Mizuno 1997). The most extensively characterized RRs of this subfamily are known to bind in tandem to DNA direct repeats (Harlocker et al. 1995; Simon et al. 1995; Blanco et al. 2002). Structural studies of two full-length members of this subfamily have indicated that the recognition helix of the effector domain is exposed to solvent in the inactive state and is not sterically hindered by the regulatory domain (Buckler et al. 2002; Robinson et al. 2003). We recently reported the crystal structure of the BeF_3^--activated regulatory domain of *E. coli* ArcA ($ArcA_N$–BeF_3^-), the first structure of an active regulatory domain from the OmpR/PhoB subfamily. Additionally, the structure of the BeF_3^--activated regulatory domain of *E. coli* PhoB (PDB ID 1ZES) has recently been solved (Bachhawat et al. 2005). Conserved features at the dimer interfaces of these RRs led us to postulate a common mechanism of activation for members of the OmpR/PhoB subfamily involving symmetric dimerization of the regulatory domains via their α4–β5–α5 faces (Bachhawat et al. 2005; Toro-Roman et al. 2005).

Two other members of the OmpR/PhoB subfamily, KdpE (Polarek et al. 1992; Walderhaug et al. 1992) and TorR (Simon et al. 1994), are the RRs of the *E. coli* TCSs KdpD–KdpE and TorS–TorR, respectively. The KdpD–KdpE TCS is involved in osmoregulation and K^+ sensing. Under K^+-limiting conditions of growth, KdpD and KdpE induce expression of the *kdpFABC* operon, which encodes the K^+-translocating Kdp-ATPase involved in high affinity K^+ uptake (Laimins et al. 1978; Rhoads et al. 1978). The TorS–TorR TCS is responsible for the tight regulation of the *torCAD* operon, which encodes the trimethylamine *N*-oxide (TMAO) reductase respiratory system in response to anaerobic conditions and the presence of TMAO (Jourlin et al. 1996). Sensing of TMAO by the unorthodox histidine kinase TorS regulates a four-step phosphorelay that results in phosphorylation of TorR and transcription of the *torCAD* operon (Jourlin et al. 1997). Induction of this operon allows *E. coli* to utilize TMAO as an additional electron acceptor during anaerobic respiration. In addition to regulating the *torCAD* operon, the TorS–TorR TCS has been shown to activate alkaline-stress defenses and repress acid-stress mechanisms in order to cope with alkalinization of the medium resulting from the reduction of TMAO to trimethylamine (Bordi et al. 2003). In this article we report the X-ray crystal structures of the regulatory domains of KdpE bound to Ca^{2+} ($KdpE_N$-Ca^{2+}) and Mg^{2+}/BeF_3^- ($KdpE_N$–BeF_3^-), and of TorR ($TorR_N$). Both $KdpE_N$ and $TorR_N$ form twofold rotationally symmetric dimers by juxtaposing their α4–β5–α5 faces. These dimerization interfaces have been analyzed and compared to those of two other OmpR/PhoB subfamily members for which structural information is available in the literature, *E. coli* $ArcA_N$–BeF_3^- (Toro-Roman et al. 2005) and *Streptococcus pneumoniae* $MicA_N$ (Bent et al. 2004).

Results and Discussion

Overall structures of $KdpE_N$ and $TorR_N$

The structures of $KdpE_N$–Ca^{2+} and $KdpE_N$–BeF_3^- were solved to a resolution of 2.0 Å and 2.2 Å, respectively, by molecular replacement methods, starting from a model of $ArcA_N$–BeF_3^- (see Materials and Methods). Initially we tried to activate $KdpE_N$ in solution using BeF_3^-, but the protein precipitated at concentrations higher than 1 mg/mL, making this an obstacle for successful crystallization. Consequently, unactivated $KdpE_N$ was used in crystallization trials. Crystals were obtained in the presence of Ca^{2+} and were subsequently used for solving the structure. Analysis of the structure revealed Ca^{2+} coordinated at the active site and the dimer conformation that we recently showed to be linked to activation in the OmpR/PhoB subfamily of RRs (Bachhawat et al. 2005; Toro-Roman et al. 2005). Indeed, trapping of OmpR/PhoB subfamily members in this dimer conformation in the absence of an activating agent during crystallization was reported for $ArcA_N$ and $MicA_N$ (Bent et al. 2004; Toro-Roman et al. 2005). Knowing that the crystals contained $KdpE_N$ dimers in an active conformation, we soaked them in solutions containing BeF_3^- with the Ca^{2+} exchanged for Mg^{2+} in order to get a complete picture of the active dimer. As expected, the crystals tolerated the addition of activating agents, and the structure was solved by molecular replacement using an alanine model of $KdpE_N$–Ca^{2+}. The $KdpE_N$–Ca^{2+} and $KdpE_N$–BeF_3^- structures contain one dimer per asymmetric unit, corresponding to a solvent content of ~50%. The two structures superimpose with an RMSD value of 0.46 Å for all C^α atoms in the dimer (see Materials and Methods).

The structure of $TorR_N$ was solved at a resolution of 1.8 Å by calculating experimental phases from a single-wavelength anomalous diffraction experiment, using selenomethionine (SeMet)-derivatized protein (see Materials

and Methods). Four $TorR_N$ molecules were found in the asymmetric unit, corresponding to two dimers, and a solvent content of ~29%. One $TorR_N$ dimer corresponds to protomers with chain IDs A and B (dimer A–B), while the second dimer corresponds to protomers C and D (dimer C–D). Just as with $KdpE_N$, the $TorR_N$ dimers are found in active conformations in the crystal structure. The two dimers in the asymmetric unit have an aligned RMSD value of 0.86 Å for all C^{α} atoms. $TorR_N$ was activated using BeF_3^- and Mg^{2+} prior to crystallization, but after solving the structure and analyzing the active sites, we noticed that no BeF_3^- and no divalent metal ion were present. We suspect that either the crystallization conditions or crystal packing might have displaced BeF_3^- from the active site. Upon examination of the crystal packing it is apparent that most of the loops in $TorR_N$, in addition to other secondary structural elements, are involved in lattice contacts. Specifically, contacts to other molecules are made by the β1–α1 loop and the β3–α3 loop of protomer A; the β1–α1 loop, the β3–α3 loop, and the β5–α5 loop of protomer B; the β1–α1 loop, the β3–α3 loop, and the β5–α5 loop of protomer C; and the β1–α1 loop and the β3–α3 loop of protomer D. These contacts result in small alterations in the positions of active site residues with the exception of Asp10, which is significantly reoriented with its side chain pointing away from the active site, incompatible with coordination to the divalent cation. Given the fact that a number of important residues within some of these loops form an integral part of the pocket where phosphorylation of the conserved aspartate occurs and that the BeF_3^- interaction is noncovalent, it is plausible that a combination of all these perturbations results in a $TorR_N$ protein that is unable to bind BeF_3^- and Mg^{2+} at the active site. We believe, nonetheless, that the overall backbone and dimer conformation is reflective of the active state of the TorR regulatory domain.

$KdpE_N$ and $TorR_N$ have the traditional $(\beta\alpha)_5$ fold of RR regulatory domains that consists of a central five-stranded parallel β-sheet surrounded by five amphipathic helices (Volz 1993) and both form symmetric dimers mediated by the α4–β5–α5 faces of their regulatory domains (Fig. 1). Each of the structures has an unusual feature that results from crystal contacts with symmetry-related molecules. In $KdpE_N$–Ca^{2+} and $KdpE_N$–BeF_3^- the active site of one protomer (chain ID A) is distorted due to the insertion of the Glu83 side chain of a symmetry-related molecule into the active site. Two conformations are observed for this Glu83: an extended conformation that reaches into the active site and another that turns away from the active site. The extended conformation of Glu83 appears to have a higher occupancy in the crystal. In the extended conformation, a carboxylate oxygen of Glu83 is positioned ~4.8 Å from the active site divalent cation, precluding the presence of a water molecule to serve as a ligand for the metal ion. In the alternate conformation, the side chain of Glu83 turns away from the active site, allowing a water molecule to coordinate to the divalent metal ion. Although weak density is observed for such a solvent molecule, it has not been included in the $KdpE_N$–Ca^{2+} and $KdpE_N$–BeF_3^- models of protomer A, as it is incompatible with the extended conformation of Glu83. In the case of $TorR_N$ each of the two dimers (A–B and C–D) contains a protomer (B and C) in which Thr80 and Tyr99 are found in conformations associated with an inactive state, even though the dimer is believed to mimic the active conformation (Fig. 1D). These two highly conserved residues (Thr/Ser and Tyr/Phe) comprise a molecular switch that modulates between inward and outward conformations primarily in response to phosphorylation or other activating influences. This crystal-induced $TorR_N$ feature will be discussed in detail in the following section.

Active sites

The site of phosphorylation in KdpE is Asp52. In $KdpE_N$–Ca^{2+} a side-chain oxygen of Asp52 forms a hydrogen bond with the main-chain nitrogen of Gly54 and also serves as one of the Ca^{2+} ligands, while the other carboxylate oxygen forms a hydrogen bond with a water molecule that is positioned where the phosphate group will be in the active state. The Ca^{2+} atom has a sevenfold coordination that can be described as a distorted pentagonal-bipyramidal geometry. The bond distances between the metal cation and its ligands range from 2.2 to 2.5 Å, typical of calcium bound to proteins. The seven Ca^{2+} ligands are provided by side-chain oxygens from Glu8, Asp9, and Asp52; three water molecules; and the main-chain carbonyl oxygen of Gly54. In addition to the conserved acidic residues Glu8 and Asp9, the other conserved active site residue Lys101 is involved in hydrogen bonds with other water molecules. All of the above interactions are depicted in Figure 2A.

The interactions found at the active site of $KdpE_N$–BeF_3^- (Fig. 2B) are analogous to those of other structures of activated RRs, all being conserved throughout different subfamilies. The Mg^{2+} cation has a sixfold coordination of octahedral geometry with bond distances between 2.1 and 2.2 Å. The ligands are provided by side-chain oxygens of Asp9 and Asp52, the main-chain carbonyl oxygen of Gly54, a fluorine of BeF_3^-, and two water molecules. The BeF_3^- molecule is noncovalently bound to the other carboxylate oxygen of Asp52. Other BeF_3^- interactions include a hydrogen bond to Ser79, a salt bridge to Lys101, and contacts with the backbone nitrogen atoms of Gly54 and Ala80. In $KdpE_N$–BeF_3^- the switch residues Ser79 and Tyr98 are in an active conformation. Relative to the positions

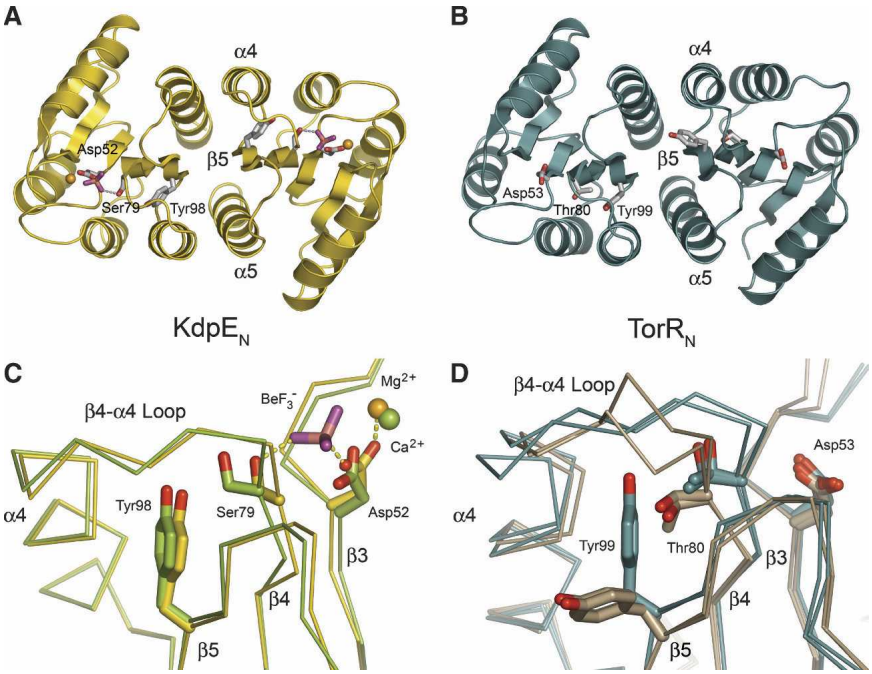

Figure 1. (*A*,*B*) Ribbon diagrams of the regulatory domains of KdpE$_N$–BeF$_3^-$ (gold) and TorR$_N$ (protomers A and B, teal). The two proteins form symmetric dimers mediated by the α4–β5–α5 faces. In KdpE$_N$–BeF$_3^-$ the side chains of Asp53, Ser79, and Tyr98 (gray and red), and BeF$_3^-$ (magenta and salmon) are shown as stick models, and the Mg^{2+} ion (orange) is shown in sphere representation. BeF$_3^-$ is noncovalently bound to the site of phosphorylation, Asp52, and serves as one of the ligands for the catalytic Mg^{2+}. Ser79 and Tyr98 are conserved residues involved in the "switch" mechanism of activation associated with phosphorylation of the conserved Asp52. The equivalent residues Asp53, Thr80, and Tyr99 are shown for TorR$_N$. (*C*) Alignment of KdpE$_N$–Ca^{2+} (protomer B, green) vs. KdpE$_N$–BeF$_3^-$ (protomer B, gold) showing the conserved residues involved in propagation of the activation signal from the active site aspartate to the α4–β5–α5 face. The side chains of Asp52, Ser79, and Tyr98 (oxygens in red), and BeF$_3^-$ (magenta and salmon) are shown in stick representation, with the Mg^{2+} (orange) and Ca^{2+} (green) ions shown as spheres. The β4–α4 loops are further stabilized into a fixed conformation by interacting with Tyr98. Minimal differences are seen between the two structures. (*D*) Alignment of the four protomers found in the asymmetric unit of the TorR$_N$ crystals. Side chains of Asp53, Thr80, and Tyr99 (oxygens in red) are shown as sticks. Two dimers are formed between protomers A–B and C–D. Protomers A and D (teal) have the switch residues Thr80 and Tyr99 in an inward active conformation, while in protomers B and C (brown) they adopt an outward conformation associated with the inactive state. The conformation of the β4–α4 loops in protomers B and C differs from that of protomers A and D because side chains of residues in these loops are used for crystal contacts.

of these residues found in inactive RR regulatory domains, Ser79 is positioned nearer to the active site, allowing coordination of its side-chain oxygen to one of the BeF$_3^-$ fluorines, concomitant with the repositioning of its neighbor, Ala80, which provides its backbone oxygen for coordination with another BeF$_3^-$ fluorine atom. Movement of Ser79 into the active site is correlated with movement of Tyr98 into an inward position where it can form a hydrogen bond with the main-chain carbonyl oxygen of Arg81, fixing and stabilizing the β4–α4 loop in an active conformation. In KdpE$_N$–Ca^{2+} Ser79 and Tyr98 are in the same active conformations, with the only difference being that Ser79 and the β4–α4 loop are ~1 Å further away from the active site as compared to their positions in KdpE$_N$–BeF$_3^-$. This displacement is clearly created by the absence of BeF$_3^-$, which attracts and interacts with atoms of Ser79 and Ala80. These small differences can be seen in Figure 1C.

TorR$_N$ has a somewhat different environment at the active site, since there is no BeF$_3^-$ or metal present (Fig. 2C). The site of phosphorylation, Asp53, is found in a fixed conformation forming a hydrogen bond to the conserved active site residue Glu9, while other interactions involving Asp53 vary depending on the protomer in the asymmetric unit. Asp53 forms a hydrogen bond with the main-chain nitrogen of Asn55 in protomers A, B, and C. Salt bridges occur between Asp53 and Lys102 in protomers B and D, and another one between Glu9 and Lys102 of protomer A. A water molecule is found at hydrogen bonding distance of one of the side-chain oxygens of Asp53 in protomers A, B, and D. The other conserved acidic residue at the active site, Asp10, is

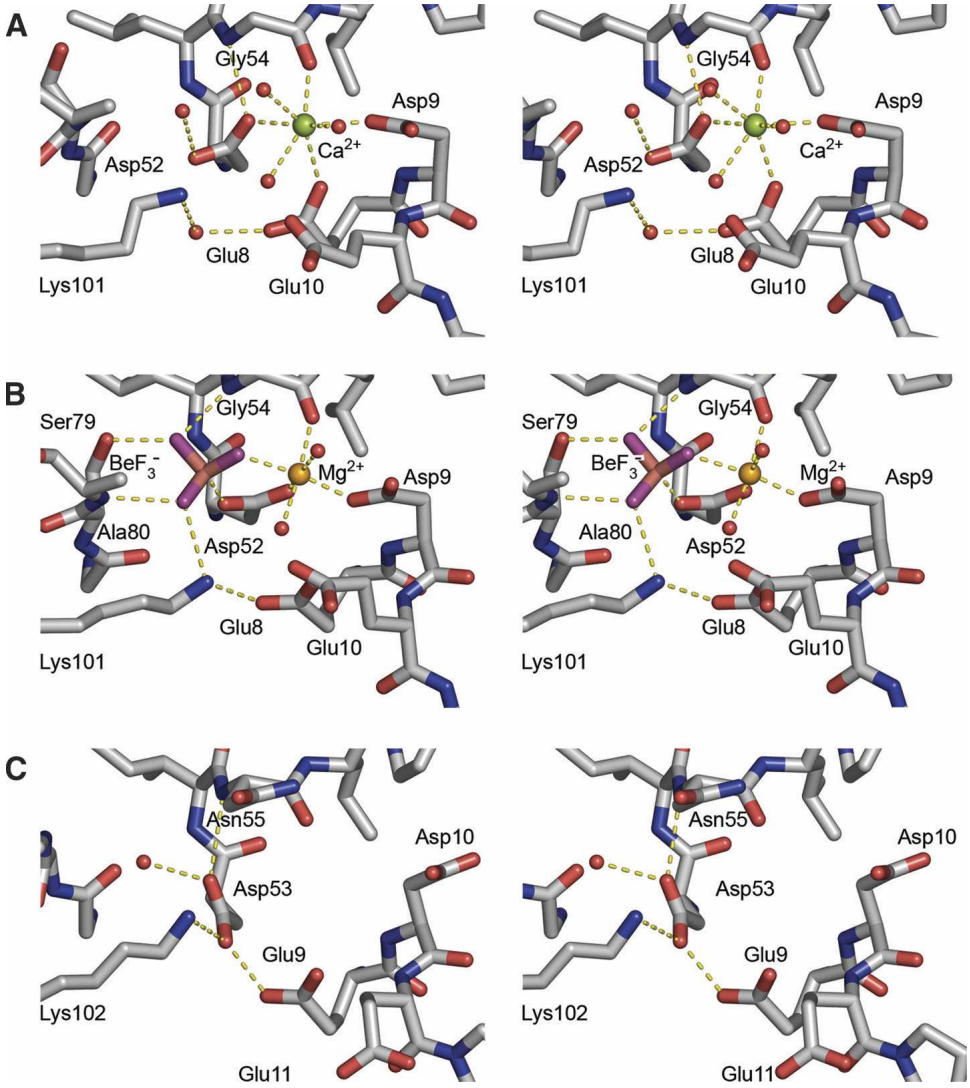

Figure 2. Stereo views of the active sites of $KdpE_N$–Ca^{2+} (*A*), $KdpE_N$–BeF_3^- (*B*), and $TorR_N$ (*C*). Carbon, oxygen, and nitrogen atoms from the protein chains are shown in gray, red, and blue, respectively. The Ca^{2+} ion, Mg^{2+} ion, and water molecules are shown as green, orange, and red spheres, respectively. (*A*) In the active site of $KdpE_N$–Ca^{2+}, the Ca^{2+} ion shows a sevenfold coordination to the side-chain oxygens of Glu8, Asp9, and Asp52; the main-chain oxygen of Gly54; and three water molecules. Lys101, which would form an ion pair with a phosphate oxygen in a phosphorylated RR, is found in a conformation pointing toward the active site and interacting with Glu8 through a water molecule bridge. (*B*) The active site of $KdpE_N$–BeF_3^- exhibits the same pattern of coordination observed in other activated structures of RR regulatory domains. The Mg^{2+} ion is octahedrally coordinated to the side-chain oxygens of Asp9 and Asp52, the main-chain oxygen of Gly54, and two water molecules. The presence of BeF_3^-, which is noncovalently bound to the phosphorylatable Asp52, induces changes in the β4–α4 loop, locking it into a particular conformation by interacting with the main-chain nitrogens of Gly54 and Ala80, and the side-chain oxygen and N^{ζ} atom of Ser79 and Lys101, respectively. (*C*) The active site of $TorR_N$, which has the phosphorylatable Asp53 side chain rotated ~90° in relation to Asp52 of $KdpE_N$, exhibits the fewest number of interactions between conserved residues. The four protomers in the asymmetric unit present slightly different interactions between Asp53 and its neighboring residues (discussed in the main text). A common feature of all four protomers is that the side chain of the conserved acidic residue Asp10 points away from the active site. The active site of protomer B is shown, in which Asp53 directly interacts with a side-chain oxygen of Glu9, the N^{ζ} atom of Lys102, the main-chain nitrogen of Asn55, and a water molecule.

found in a conformation that points away from the active site. Asp10 is involved in the coordination of the metal cation at the active site. In protomer A Asp10 forms a hydrogen bond with the main-chain carbonyl oxygen of Ala33 (β2–α2 loop), while in protomer B Asp10 forms a hydrogen bond with the main-chain nitrogen of Pro2 from a neighboring molecule (the initiator methionine had been post-translationally

removed). In protomers C and D, Asp10 does not make any contacts and is simply pointing away to the solvent. A similar orientation for this residue was seen in the crystal structure of Spo0F (PDB ID 1NAT; Madhusudan et al. 1997). In the structure of Spo0F, the corresponding Asp11 residue points away from the active site and into the solvent without making any crystal contacts. Binding of a metal cation promotes movement of the Asp11 side chain of Spo0F into the active site to form the cation cavity. The absence of the metal cation could be a reason the side chain of Asp10 is oriented away from the active site in $TorR_N$.

In the previous section it was mentioned that protomers B and C of the $TorR_N$ A–B and C–D dimers contain the two switch residues, Thr80 and Tyr99, in conformations representative of the inactive state, while in protomers A and D they exist in an active conformation. Examination of the environment around these residues, mainly the β4–α4 loop, provides some clues as to why these residues in one of the protomers of each dimer are found in an inactive conformation. The β4–α4 loop, which is mainly composed of residues 81–85, is clearly being pulled away from its expected active conformation in order to participate in contacts with symmetry-related molecules in the lattice. These interactions move the loop to a conformation away from the active site (Fig. 1D). The displacement is especially critical for the C^{α} atom of Thr80, which moves ~2.0 Å away from the active site and toward Tyr99. This appears to promote a change in the conformation of Thr80 to an outward position, with its side chain oriented away from the active site. Consequently, Tyr99 must adopt an outward conformation to avoid steric collision with the outward conformation of Thr80. It is likely that in the absence of crystal contacts, the β4–α4 loop and the switch residues, Thr80 and Tyr99, would be found in an active conformation as observed in the other two protomers in the asymmetric unit.

Common dimer interface

Both $KdpE_N$ and $TorR_N$ form symmetric dimers that are mediated by their α4–β5–α5 faces. In both cases the dimers are found in the asymmetric units of the crystals. The average total surface area buried at the dimer interface for $KdpE_N$ and $TorR_N$ is 1800 $Å^2$ (900 $Å^2$ per monomer) and 2000 $Å^2$ (1000 $Å^2$), respectively. As in the recently reported structure of $ArcA_N$–BeF_3^-, the interfaces of $KdpE_N$–BeF_3^- and $TorR_N$ are mediated by a hydrophobic patch that packs the α4 helix of one monomer against the α5 helix of the other. A network of salt bridges and other electrostatic interactions confer additional stability to the interface. The majority of these interactions involve residues that are highly conserved in the OmpR/PhoB subfamily of RRs. Since $KdpE_N$–Ca^{2+} and $KdpE_N$–BeF_3^- have identical interfaces, we will use $KdpE_N$ to refer to both structures within this section.

In $KdpE_N$ the core of the hydrophobic patch is formed by Ile88 (α4), Leu91 (α4), Ala110 (α5), and Val114 (α5), with additional contributions from the aliphatic portions of the side chains Glu84 (α4), Lys87 (α4), Glu107 (α5), and Arg111 (α5) (Fig. 3A). Val114 is not part of the group of highly conserved residues, and, as a result, extends the hydrophobic patch further down the helices when compared to $ArcA_N$–BeF_3^-, which has an asparagine at that site. The conserved intermolecular electrostatic interactions are formed between Asp97 (β5) and Arg111 (α5), Asp96 (α4–β5 loop) and Arg118 (α5), and Asp92 (α4) and Arg113 (α5) (Fig. 3B). Arg111 is further stabilized by an additional intramolecular salt bridge to Glu107 (α5). In addition, the guanidinium group of Arg117 (α5) forms two intermolecular hydrogen bonds to the main-chain carbonyl oxygens of Ala95 (α4–β5 loop) and Leu91 (α4). This interaction of Arg117 is equivalent to the one achieved by the side-chain nitrogen of Asn116 (α5) in $ArcA_N$–BeF_3^- with the exception that Asn116 is found one helical turn above Arg117 of $KdpE_N$, compensating for its shorter side chain. In both cases the interaction results in additional stabilization of the α4–β5 loop.

The dimer interface of $TorR_N$, like that of $KdpE_N$, has the same conserved interactions observed in $ArcA_N$–BeF_3^- with the exception of the switch tyrosine (Tyr99, protomers B and C), which in the outward conformation interferes with some of the interactions. The hydrophobic patch is composed of Ile89 (α4), Leu92 (α4), and Val111 (α5), with further contributions from the side-chain aliphatic portions of Glu108 (α5) and Arg112 (α5) (Fig. 3C). Intermolecular salt bridges include Arg88 (α4)–Glu108 (α5), Asp98 (β5)–Arg112 (α5), and Asp97 (α4–β5 loop)–Arg119 (α5) (Fig. 3D). On one side of the interface the outwardly oriented side chain of Tyr99 (β5) bridges the interaction between Glu108 and Arg88. The other two residues that are typically involved in conserved intermolecular salt bridges at the outer side of the interface, Glu93 (α4) and Lys114 (α5), are instead involved in contacts with nearby molecules related by crystal symmetry. Also present in $TorR_N$ are the analogous intermolecular hydrogen bonds between the side-chain nitrogen of Asn115 (α5) and the main-chain carbonyl oxygens of Leu92 (α4) and Ala96 (α4–β5 loop) found in $KdpE_N$ and $ArcA_N$–BeF_3^-. In $TorR_N$ this interaction is identical to the one that exists in $ArcA_N$–BeF_3^-.

Another common feature of the dimer interfaces, including those of $ArcA_N$ and $MicA_N$, is that the α5 arginine residue involved in the lower salt bridge to the α4–β5 loop aspartate is stabilized in its position by a

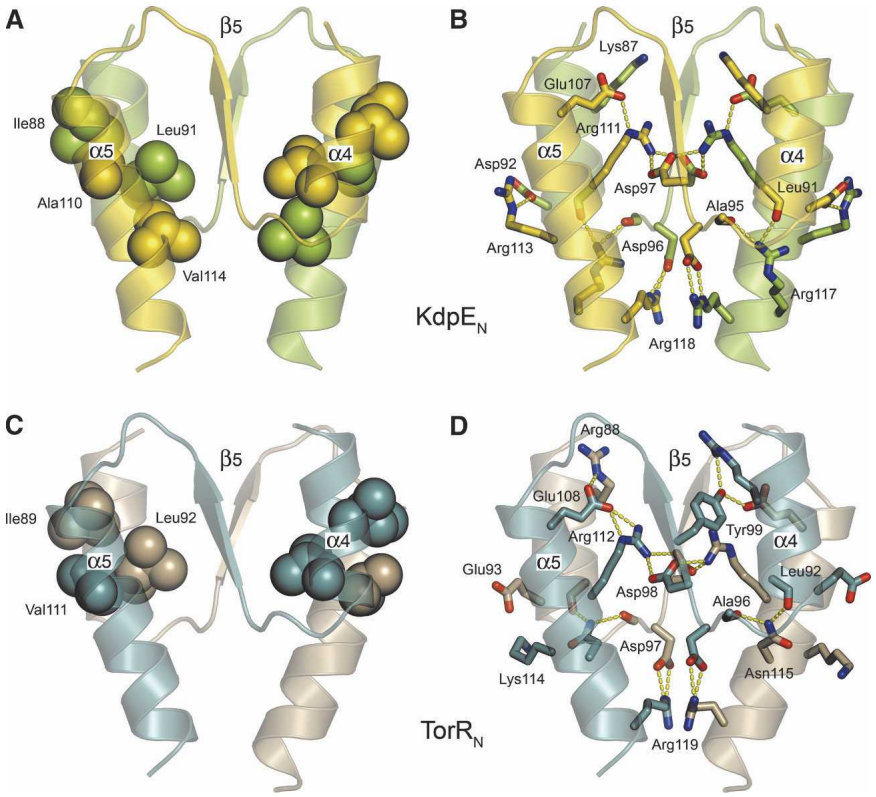

Figure 3. Conserved intermolecular interactions of $KdpE_N$–BeF_3^- (*A*,*B*) and $TorR_N$ (*C*,*D*) at the dimer interface. $KdpE_N$–BeF_3^- protomers are distinguished by the colors gold and green, and $TorR_N$, by the colors teal and brown. Hydrophobic and electrostatic interactions are represented by sphere and stick models, respectively. (*A*,*C*) In both $KdpE_N$–BeF_3^- and $TorR_N$, the α4 and α5 helices are packed together through a conserved hydrophobic patch formed in $KdpE_N$–BeF_3^- by Ile88 (α4), Leu91 (α4), Ala110 (α5), and Val114 (α5). Analogous conserved interactions are seen in $TorR_N$ except for an additional nonconserved hydrophobic residue in $KdpE_N$–BeF_3^- (Val114) that further extends the hydrophobic patch down the path of the helices. (*B*,*D*) The interface of these dimers is further stabilized by a network of inter- and intramolecular salt bridges formed in $KdpE_N$–BeF_3^- by Glu107 (α5) and Arg111 (α5), Asp97 (β5) and Arg111 (α5), Asp96 (α4–β5 loop) and Arg118 (α5), Asp92 (α4) and Arg113 (α5), and Ala95 (α4–β5 loop)/Leu91 (α4) and Arg117 (α5). In $TorR_N$ the interactions are formed between Glu108 (α5) and Arg88 (α4), Glu108 (α5) and Arg112 (α5), Asp98 (β5) and Arg112 (α5), Asp97 (α4–β5 loop) and Arg119 (α5), and Ala96 (α4–β5 loop)/Leu92 (α4) and Asn115 (α5). On the right side of the $TorR_N$ interface the Glu108–Arg88 interaction is bridged by the side-chain oxygen of Tyr99, which is found in an outward conformation in protomers B and C (see Fig. 1D). The side chains of Glu93 and Lys114 are involved in crystal contacts, and thus do not form the analogous salt bridge seen in $KdpE_N$–BeF_3^-.

small, highly electrostatic pocket (Fig. 4). This pocket is formed by main-chain atoms of Ala72, Val73, Val75 (all part of the α3–β4 loop), and Gly94 (α4–β5 loop), and side chain atoms of Arg68 (α3) and Asp96 (α4–β5 loop), using the sequence numbering of KdpE (Fig. 4A). The long, positively-charged side chain of Arg68 is also highly conserved as either arginine or lysine. Superimposing all four dimers together shows an identical environment for the main-chain and side-chain atoms involved in electrostatic interactions at this site (Fig. 4B).

Symmetric dimerization as a mechanism of activation

The DNA-binding domains of OmpR/PhoB subfamily RRs are known to bind in tandem to DNA direct repeats (Harlocker et al. 1995; Simon et al. 1995; Blanco et al. 2002). Structural analyses of two inactive full-length OmpR/PhoB RRs have shown the recognition helix of the DNA-binding domain to be solvent-exposed and accessible to DNA (Buckler et al. 2002; Robinson et al. 2003). Additional biochemical data indicate a role for dimerization or oligomerization in the regulation of activities of RRs of the OmpR/PhoB subfamily (Fiedler and Weiss 1995; McCleary 1996; Liu and Hulett 1997; Wösten and Groisman 1999; Robinson et al. 2003; Toro-Roman et al. 2005), especially for RRs that utilize multiple tandem binding sites. The common dimerization mode of the active regulatory domains of KdpE, TorR, ArcA, and MicA are reflected in the conservation of surface residues within their α4–β5–α5 faces (Fig. 5).

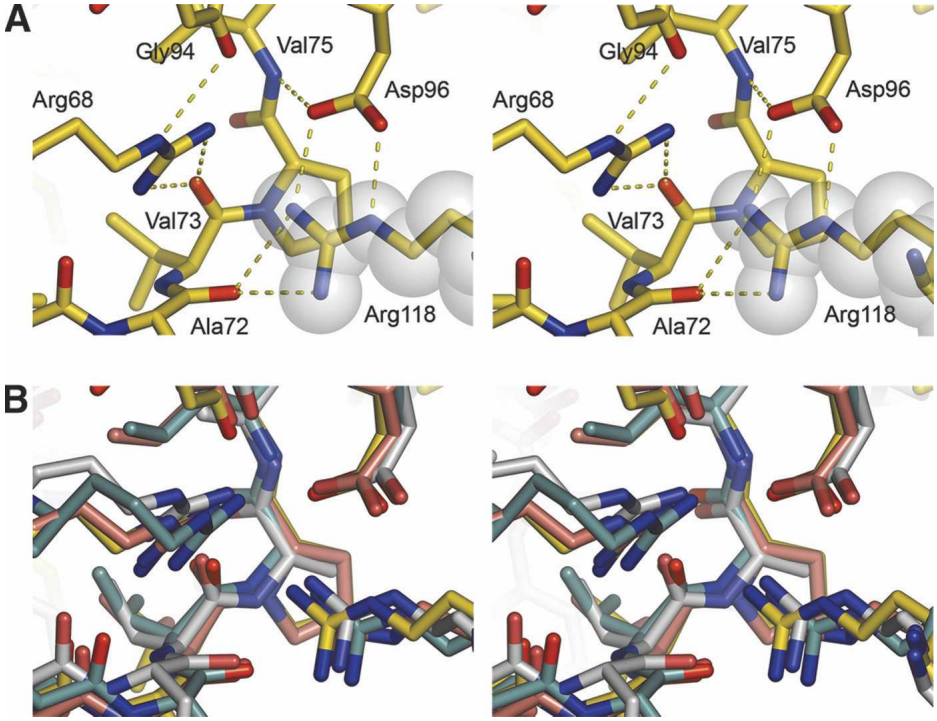

Figure 4. Stereo views of the environment surrounding the conserved arginine involved in the lower intermolecular salt bridge. Protein atoms are shown in stick representation with oxygen and nitrogen atoms in red and in blue, respectively. (*A*) A region of $KdpE_N$–BeF_3^- (gold) showing the Arg118 of one protomer (superimposed with white spheres) positioned within an electrostatic pocket formed by the second protomer of the dimer. The pocket is mainly created by electrostatic interactions between atoms of residues Arg68, Ala72, Val73, Val75, Gly94, and Asp96. (*B*) Structural alignment of dimers of $KdpE_N$–BeF_3^- (gold), $TorR_N$ (A–B dimer, teal), *E. coli* $ArcA_N$–BeF_3^- (PDB ID 1XHF, gray) and *S. pneumoniae* $MicA_N$ (PDB ID 1NXW, salmon). The tertiary structure of the pocket is highly conserved, with identical positioning of the atoms involved in electrostatic interactions. The position of the side chain of the arginine from the adjacent protomer is also conserved.

We have previously noted in the analysis of $ArcA_N$–BeF_3^- that the residues mediating the dimer interface are highly conserved throughout OmpR/PhoB subfamily members, but are not conserved in RRs of other subfamilies. Based on this sequence conservation and similar dimer structures of several activated regulatory domains, we have postulated that most all OmpR/PhoB RRs adopt similar structures in their activated states. We envision that upon phosphorylation, conformational changes in the α4–β5–α5 face disrupt any interfaces that may exist between the regulatory and DNA-binding domains in the inactive states. The two domains separate, allowing the regulatory domains to dimerize with a rotationally symmetric orientation using their α4–β5–α5 faces. The DNA-binding domains, attached via flexible linkers, are free to adopt a tandem arrangement or, theoretically, any arrangement dictated by DNA recognition sites and/or intrinsic protein/protein interaction surfaces.

Some of the OmpR/PhoB subfamily members, for example, TorR, are capable of binding to their recognition sequences in vitro in the absence of phosphorylation (Simon et al. 1995). One proposed model for the regulation of *torC*, the first gene of the *torCAD* operon that encodes a membrane-anchored c type cytochrome (Bragg and Hackett 1983; Iobbi-Nivol et al. 1994), involves the hierarchical binding of TorR to four different *tor* boxes. Boxes one and two are considered to be high affinity binding sites while boxes three and four are regarded as low affinity binding sites. The first two high affinity boxes are capable of binding an unphosphorylated dimer of TorR while the last two can only be occupied by phosphorylated TorR. Phosphorylation could then promote intermolecular interactions between TorR dimers enhancing or increasing the affinity of TorR for boxes three and four, thus forming an oligomer that has a more stable interaction with DNA. This kind of situation in which the protein binds to DNA prior to phosphorylation, if occurring in vivo, could be attributed to formation of an active dimer conformation induced by protein concentration as a result of localization, the presence of DNA, or the intracellular conditions during signaling. The ability of $KdpE_N$, $TorR_N$, $ArcA_N$, and $MicA_N$ to crystallize as active dimers at high concentrations even in the absence of activating agents supports this view.

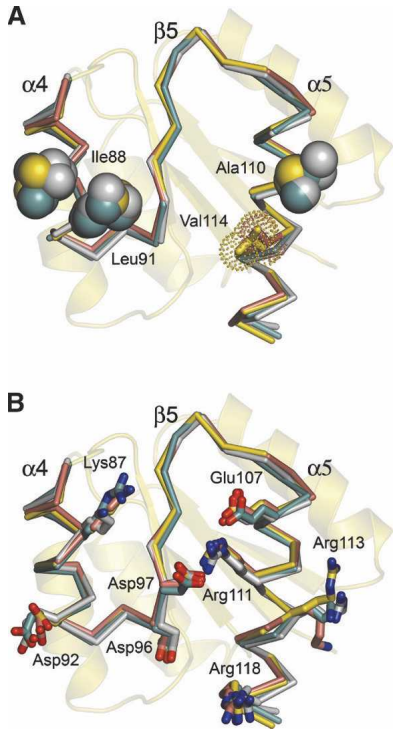

Figure 5. Alignment of single protomers showing the conservation of residues that mediate the α4–β5–α5 dimer interface in active RRs of the OmpR/PhoB subfamily. The α4–β5–α5 faces of $KdpE_N$–BeF_3^- (protomer A, gold), $TorR_N$ (protomer B, teal), *E. coli* $ArcA_N$–BeF_3^- (protomer A, PDB ID 1XHF, gray), and *S. pneumoniae* $MicA_N$ (PDB ID 1NXW, salmon) are depicted as C^α traces. Sequence numbering is for KdpE. (*A*) Conservation of hydrophobic residues (spheres) that make up the hydrophobic patch. Dotted spheres represent hydrophobic residues that extend the conserved hydrophobic patch along the two helices but are not fully conserved in *E. coli* OmpR/PhoB subfamily RRs, among which nine of 15 have a hydrophobic residue at this position. (*B*) Conservation of residues involved in formation of electrostatic interactions (sticks). All residue side chains superimpose well with the exception of those that are situated at the periphery of the proteins and are more susceptible to solvation or formation of crystal contacts. In $TorR_N$ and $MicA_N$, the equivalent residues of the $KdpE_N$ Asp92–Arg113 salt bridge are used for crystal contacts.

In summary, we have determined the structures of the activated regulatory domains of KdpE and TorR, both members of the highly populated OmpR/PhoB subfamily of RRs. These two structures provide further evidence for a common mechanism of activation and regulation by dimerization for members of this subfamily. Variations on the basic scheme can provide complexity to specific systems. Greater complexity can presumably be achieved by introduction of additional nonconserved intermolecular interactions during oligomerization in either inactive or active states, variation in the number and sequences of binding sites that regulate an operon, the presence of additional binding sites for heterologous transcription factors, and variation in the length of the linkers that tether the regulatory and DNA-binding domains of the RRs.

Materials and methods

Expression and purification

A DNA fragment encoding $KdpE_N$, residues 1–121 with an A121Q substitution at the C-terminal residue, was PCR amplified from pEF33, which contains full-length *E. coli kdpE*, and subcloned into the T7 vector pJES307 (Tabor and Richardson 1985) at the NdeI and BamHI polylinker sites to create pEF27. Plasmid pEF27 was transformed into *E. coli* BL21(DE3) (Novagen). Cells were grown at 37°C in Luria-Bertani medium with the addition of ampicillin to a final concentration of 100 μg/mL. $KdpE_N$ was overexpressed by induction with 0.5 mM isopropyl-β-D-thiogalactopyranoside followed by incubation for 3 h. All subsequent steps were carried out at 4°C. Cells were harvested by centrifugation, washed with 50 mM Tris-Cl, 300 mM NaCl, 1 mM dithiothreitol, and 1 mM EDTA (pH 8.0), and lysed by sonication in the same buffer. The lysate was clarified by ultracentrifugation for 60 min at 80,000*g*. The soluble portion of the lysate was fractionated by addition of a saturated solution of $(NH_4)_2SO_4$ to 40% saturation. The pellet was resuspended and dialyzed overnight in 25 mM Tris-Cl (pH 8.5) (buffer A). The protein sample was loaded onto two tandem 5-mL HiTrap Q Sepharose columns (GE Health Care) and eluted with a 150-mL gradient of 0.10–0.50 M NaCl in buffer A. Fractions containing $KdpE_N$ were pooled and the HiTrap Q chromatographic step was repeated a second time as described. After we pooled the fractions containing $KdpE_N$, the sample was precipitated by addition of a saturated solution of $(NH_4)_2SO_4$ to 40% saturation, resuspended in 25 mM Tris-Cl and 100 mM NaCl (pH 7.5) (buffer B), and subjected to gel filtration chromatography on a Superdex75 26/60 gel filtration column (GE Health Care) equilibrated in buffer B.

A DNA fragment encoding $TorR_N$, residues 1–122 with a L122Q substitution at the C-terminal residue, was PCR-amplified from pEF32, which contains full-length *E. coli torR*, and subcloned into pJES307 at the NdeI and BamHI polylinker sites to create pEF26. Plasmid pEF26 was transformed into the methionine auxotroph strain B834(DE3)-pLysS (Novagen) for production of SeMet-substituted $TorR_N$. The cell growth procedure was modified from Hendrickson et al. (1990) and described elsewhere (Robinson et al. 2002) with the cell culture being incubated overnight at 25°C after induction with 0.5 mM isopropyl-β-D-thiogalactopyranoside. Sonication and ultracentrifugation of SeMet $TorR_N$ was performed as described above for $KdpE_N$ with inclusion of 10 mM β-mercaptoethanol (βME) in all solutions. The lysate was fractionated by addition of a saturated solution of $(NH_4)_2SO_4$ to 25% saturation. The pellet was resuspended and dialyzed overnight in 25 mM Tris-Cl and 10 mM βME (pH 8.0) (buffer C). The protein sample was loaded onto two tandem 5-mL HiTrap Q columns and eluted with a 400-mL gradient of 0–2.0 M NaCl in buffer C. Fractions containing SeMet $TorR_N$ were pooled, precipitated with a saturated solution of $(NH_4)_2SO_4$ to 40% saturation, resuspended in 25 mM Tris-Cl, 100 mM NaCl, and 10 mM βME (pH 8.0) (buffer D), and subjected to gel filtration on a Superdex75 26/60 column equilibrated in buffer D.

Crystallization and data collection

Purified $KdpE_N$ and SeMet $TorR_N$ were dialyzed overnight into 50 mM Tris-Cl (pH 8.4), with the addition of 10 mM βME to SeMet $TorR_N$. Both protein samples were concentrated at 4°C with Biomax-10 concentrators to 25–35 mg/mL as determined by absorbance at 280 nm. All crystals were grown at 20°C using the hanging drop vapor diffusion method. Orthorhombic $KdpE_N$ crystals containing one dimer in the asymmetric unit grew in 10% polyethylene glycol 8000, 0.1 M 2-morpholinoethanesulfonic acid (pH 6.0), and 0.1 M calcium acetate. Cryoprotection was achieved by sequential transfer of crystals into six solutions containing reservoir solution in addition to ethylene glycol in increments of 5% to a final concentration of 30% ethylene glycol. Crystals were frozen in a 100 K nitrogen stream. $KdpE_N$ was found to precipitate when BeF_3^- was added to the solution at protein concentrations higher than 1 mg/mL. To obtain the BeF_3^--bound data set, apo-$KdpE_N$ crystals were transferred into a fresh reservoir solution containing 5.3 mM $BeCl_2$ and 33 mM NaF, in which the 0.1 M calcium acetate had been replaced with 0.1 M $MgCl_2$, and were incubated for 3 h. Monoclinic SeMet $TorR_N$ crystals containing two dimers per asymmetric unit grew in 26% polyethylene glycol 2000 monomethyl ether, 0.4 M $(NH_4)_2SO_4$, 0.1 M sodium acetate trihydrate (pH 6.0), and 1%–3% glycerol. Crystals were cryoprotected by sequential transfer into four solutions containing reservoir solution in addition to glycerol in increments of 5% to a final concentration of 20% glycerol. Crystals were frozen in a 100 K nitrogen stream. Although SeMet $TorR_N$ crystals were grown in the presence of BeF_3^-, there was no indication of incorporation into the active site (see Results and Discussion).

$KdpE_N$–Ca^{2+} and $KdpE_N$–BeF_3^- native data sets were each collected from a single crystal grown over a period of 2–3 d. A second $KdpE_N$–Ca^{2+} data set was collected from the same crystal with the use of a beam attenuator to properly measure overloaded low-resolution reflections obtained in the first data set. A SeMet TorR multiwavelength anomalous diffraction data set was collected from a single crystal grown in ~1 wk. Data sets were collected at beamline X4A at the National Synchrotron Light Source at Brookhaven National Laboratory. All data were processed and scaled with DENZO and SCALEPACK (Otwinowski and Minor 1997). Details and statistics for each data set are listed in Table 1.

Structure determination and refinement

The structure of $KdpE_N$–Ca^{2+} was solved by molecular replacement (Rossman 1990) with Phaser 1.2 (Storoni et al. 2004)

Table 1. *Data collection and refinement statistics*

Data set	$KdpE_N$-Ca^{2+}	$KdpE_N$-BeF_3^-	SeMet[a] $TorR_N$
Data collection			
Space group	$C222_1$	$C222_1$	$P2_1$
Wavelength (Å)	1.07179	1.07179	0.97888
Resolution limits (Å)	30.0–2.00 (2.07–2.00)	30.0–2.20 (2.28–2.20)	20.0–1.80 (1.86–1.80)
Unit-cell parameters			
a, b, c (Å)	70.37, 127.16, 65.21	70.91, 126.68, 62.66	55.47, 58.39, 64.09
β (°)	—	—	112.25
No. of reflections	20,163	14,572	34,815
Completeness (%)	100 (99.9)	96.8 (88.9)	97.7 (80.4)
R_{sym}[b]	0.063 (0.159)	0.048 (0.213)	0.084 (0.367)
$I/\sigma(I)$	48.0 (24.2)	30.1 (7.8)	20.9 (3.3)
Mosaicity	0.26	0.99	0.50
Redundancy	13.6 (10.2)	5.4 (4.9)	7.0 (4.7)
Refinement			
Resolution limits (Å)	30.0–2.00 (2.05–2.00)	30.0–2.20 (2.36–2.20)	20.0–1.80 (1.85–1.80)
No. of protein monomers[c]	2	2	4
No. of protein atoms	1869	1866	3750
No. of solvent molecules	160	117	213
No. of metal cations	2 (Ca^{2+})	2 (Mg^{2+})	—
No. of reflections (work/test)	18,100/2046	13,343/706	30,446/3310
R_{cryst} /R_{free}[d]	0.193/0.242	0.227/0.265	0.192/0.244
RMSD bond length (Å)	0.017	0.017	0.010
RMSD bond angle (°)	1.556	1.653	1.224
Mean temperature factor (Å^3)	25.05	45.01	22.47
Solvent content (%)	54.2	52.5	28.8
Ramachandran plot			
Most favored (%)	96.7	93.8	95.2
Additionally allowed (%)	3.3	6.2	4.8
Disallowed	None	None	None

Values in parentheses correspond to the highest resolution shell.
[a] Selenomethionine-substituted protein.
[b] $R_{sym} = \sum|I_{obs} - I_{avg}|/\sum I_{avg}$
[c] Protein monomers in the asymmetric unit.
[d] R factor $= \sum||F_{obs}|_{(hkl)} - |F_{calc}|_{(hkl)}|/\sum|F_{obs}|_{(hkl)}$

using a polyalanine model of $ArcA_N$–BeF_3^- (PDB ID 1XHF) lacking the α3–β4, β4–α4, and β5–α5 loops. Iterative cycles of density modification and refinement were performed automatically applying solvent flattening, histogram matching, and twofold noncrystallographic symmetry (NCS) averaging using Refmac 5.1.24 (Murshudov et al. 1997) and DM (Cowtan 1994) as implemented in NCSref from the CCP4 4.2.2 package (Collaborative Computational Project, No. 4 1994). The resulting 2.0 Å averaged map was of excellent quality, revealing density of missing loops and side chains. Model building and refinement were performed in XtalView (McRee 1999) and Refmac starting with tight NCS restraints that were gradually released until convergence. Waters were located using ARP_WATERS (Lamzin and Wilson 1993) and by manual inspection. The final model of $KdpE_N$–Ca^{2+} includes residues 2–121 and 1–120 of chains A and B, respectively, with a final R_{cryst} of 0.193 and R_{free} of 0.242. $KdpE_N$–BeF_3^- was solved by molecular replacement with Phaser using a polyalanine model of $KdpE_N$–Ca^{2+}. Density modification, model building, and refinement to a resolution of 2.2 Å were performed as in $KdpE_N$–Ca^{2+} by using CNS 1.1 (Brünger et al. 1998) and Refmac. The final model of $KdpE_N$–BeF_3^- includes residues 1–121 and 1–120 of chains A and B, respectively, with a final R_{cryst} of 0.227 and R_{free} of 0.265.

The structure of $TorR_N$ was solved by single-wavelength anomalous diffraction phasing using CNS with 11 out of 16 possible selenium sites found corresponding to four molecules in the asymmetric unit. The reflections were phased to a resolution of 1.8 Å using CNS, and an initial interpretable map was obtained through density modification by phase extension with solvent flattening, histogram matching, and twofold NCS averaging (two dimers as NCS units) as implemented in DM. A single protomer was manually traced using XtalView and subsequently was used to place the remaining three protomers in the asymmetric unit using Phaser. Model building and refinement were completed as in $KdpE_N$-Ca^{2+}. Analysis of the structure revealed that the initiator methionine had been post-translationally removed, as the N terminus of the second amino acid in the sequence, Pro2, was found too close to and interacting with other symmetry-related molecules. The final model of $TorR_N$ includes residues 2–122, 2–121, 2–121, and 2–121 of chains A, B, C, and D, respectively, with a final R_{cryst} of 0.192 and R_{free} of 0.244.

Data quality and structure stereochemistry for the three structures were validated using the programs SFCHECK (Vaguine et al. 1999) and PROCHECK (Laskowski et al. 1993), respectively. All structures show no residues in disallowed regions of the Ramachandran plot. Details and statistics for each data set are listed in Table 1. All figures were created using the molecular visualization program PyMOL (http://pymol.sourceforge.net/).

Structural alignments and calculation of RMSD values

Structural alignments shown in Figures 1 (C and D), 4 (B), and 5 (A and B) were produced using PyMOL's built-in fitting algorithm. Reported RMSD values for alignment of C^α atoms between $KdpE_N$–Ca^{2+} and $KdpE_N$–BeF_3^- dimers and between $TorR_N$ dimers in the asymmetric unit were calculated using the program LSQKAB (Kabsch 1976) from the CCP4 package.

Protein Data Bank data deposition

Atomic coordinates and structure factors have been deposited in the Protein Data Bank (Berman et al. 2000) with PDB ID codes 1ZH2, 1ZH4, and 1ZGZ for the $KdpE_N$–Ca^{2+}, $KdpE_N$–BeF_3^-, and $TorR_N$ structures, respectively.

Acknowledgments

We thank E. Fox for technical assistance with construction of expression vectors and the staff at beamline X4A at the National Synchrotron Light Source at Brookhaven National Laboratory for technical assistance. This work was supported by grant R37GM047958 from the NIH. A.T.R. was supported by NIH grants T32GM08319 and 5F31GM070142 (NRSA-MARC). A.M.S. is an investigator of the Howard Hughes Medical Institute.

References

Bachhawat, P., Swapna, G.V.T., Montelione, G.T., and Stock, A.M. 2005. Mechanism of activation for transcription factor PhoB suggested by different modes of dimerization in the inactive and active states. *Structure (Camb.)* **13:** 1353–1363.

Bent, C.J., Isaacs, N.W., Mitchell, T.J., and Riboldi-Tunnicliffe, A. 2004. Crystal structure of the response regulator 02 receiver domain, the essential YycF two-component system of *Streptococcus pneumoniae* in both complexed and native states. *J. Bacteriol.* **186:** 2872–2879.

Berman, H.M., Westbrook, J., Feng, Z., Gilliland, G., Bhat, T.N., Weissig, H., Shindyalov, I.N., and Bourne, P.E. 2000. The Protein Data Bank. *Nucleic Acids Res.* **28:** 235–242.

Blanco, A.G., Sola, M., Gomis-Ruth, F.X., and Coll, M. 2002. Tandem DNA recognition by PhoB, a two-component signal transduction transcriptional activator. *Structure (Camb.)* **10:** 701–713.

Bordi, C., Theraulaz, L., Mejean, V., and Jourlin-Castelli, C. 2003. Anticipating an alkaline stress through the Tor phosphorelay system in *Escherichia coli*. *Mol. Microbiol.* **48:** 211–223.

Bragg, P.D. and Hackett, N.R. 1983. Cytochromes of the trimethylamine *N*-oxide anaerobic respiratory pathway of *Escherichia coli*. *Biochim. Biophys. Acta* **725:** 168–177.

Brünger, A.T., Adams, P.D., Clore, G.M., DeLano, W.L., Gros, P., Grosse-Kunstleve, R.W., Jiang, J.S., Kuszewski, J., Nilges, M., Pannu, N.S., et al. 1998. Crystallography & NMR system: A new software suite for macromolecular structure determination. *Acta Crystallogr. D Biol. Crystallogr.* **54:** 905–921.

Buckler, D.R., Zhou, Y., and Stock, A.M. 2002. Evidence of intradomain and interdomain flexibility in an OmpR/PhoB homolog from *Thermotoga maritima*. *Structure (Camb.)* **10:** 153–164.

Chabre, M. 1990. Aluminofluoride and beryllofluoride complexes: New phosphate analogs in enzymology. *Trends Biochem. Sci.* **15:** 6–10.

Cho, H., Wang, W., Kim, R., Yokota, H., Damo, S., Kim, S.-H., Wemmer, D.E., Kustu, S., and Yan, D. 2001. BeF_3^- acts as a phosphate analog in proteins phosphorylated on aspartate: Structure of a BeF_3^- complex with phosphoserine phosphatase. *Proc. Natl. Acad. Sci.* **98:** 8525–8530.

Collaborative Computational Project, No. 4. 1994. The CCP4 suite: Programs for protein crystallography. *Acta Crystallogr. D Biol. Crystallogr.* **50:** 760–763.

Cowtan, K. 1994. "DM": An automated procedure for phase improvement by density modification. *Joint CCP4 and ESF-EACBM Newsletter on Protein Crystallography* **31:** 34–38.

Fiedler, U. and Weiss, V. 1995. A common switch in activation of the response regulators NtrC and PhoB: Phosphorylation induces dimerization of the receiver modules. *EMBO J.* **14:** 3696–3705.

Harlocker, S.L., Bergstrom, L., and Inouye, M. 1995. Tandem binding of six OmpR proteins to the *ompF* upstream regulatory sequence of *Escherichia coli*. *J. Biol. Chem.* **270:** 26849–26856.

Hendrickson, W.A., Horton, J.R., and LeMaster, D.M. 1990. Selenomethionyl proteins produced for analysis by multiwavelength

anomalous diffraction (MAD): A vehicle for direct determination of three-dimensional structure. *EMBO J*. **9:** 1665–1672.
Iobbi-Nivol, C., Crooke, H., Griffiths, L., Grove, J., Hussain, H., Pommier, J., Mejean, V., and Cole, J.A. 1994. A reassessment of the range of *c*-type cytochromes synthesized by *Escherichia coli* K-12. *FEMS Microbiol. Lett*. **119:** 89–94.
Jourlin, C., Bengrine, A., Chippaux, M., and Mejean, V. 1996. An unorthodox sensor protein (TorS) mediates the induction of the *tor* structural genes in response to trimethylamine *N*-oxide in *Escherichia coli*. *Mol. Microbiol*. **20:** 1297–1306.
Jourlin, C., Ansaldi, M., and Mejean, V. 1997. Transphosphorylation of the TorR response regulator requires the three phosphorylation sites of the TorS unorthodox sensor in *Escherichia coli*. *J. Mol. Biol*. **267:** 770–777.
Kabsch, W. 1976. A solution for the best rotation to relate two sets of vectors. *Acta Crystallogr. A* **32:** 922–923.
Kleerebezem, M., Quadri, L.E., Kuipers, O.P., and de Vos, W.M. 1997. Quorum sensing by peptide pheromones and two-component signal-transduction systems in Gram-positive bacteria. *Mol. Microbiol*. **24:** 895–904.
Laimins, L.A., Rhoads, D.B., Altendorf, K., and Epstein, W. 1978. Identification of the structural proteins of an ATP-driven potassium transport system in *Escherichia coli*. *Proc. Natl. Acad. Sci*. **75:** 3216–3219.
Lamzin, V.S. and Wilson, K.S. 1993. Automated refinement of protein models. *Acta Crystallogr. D Biol. Crystallogr*. **49:** 129–147.
Laskowski, R.A., McArthur, M.W., Moss, D.S., and Thornton, J.M. 1993. PROCHECK: A program to check the stereochemical quality of protein structures. *J. Appl. Crystallogr*. **26:** 282–291.
Liu, W. and Hulett, F.M. 1997. *Bacillus subtilis* PhoP binds to the *phoB* tandem promoter exclusively within the phosphate starvation-inducible promoter. *J. Bacteriol*. **179:** 6302–6310.
Lukat, G.S. and Stock, J.B. 1993. Response regulation in bacterial chemotaxis. *J. Cell. Biochem*. **51:** 41–46.
Madhusudan, M., Zapf, J., Hoch, J.A., Whiteley, J.M., Xuong, N.H., and Varughese, K.I. 1997. A response regulatory protein with the site of phosphorylation blocked by an arginine interaction: Crystal structure of Spo0F from *Bacillus subtilis*. *Biochemistry* **36:** 12739–12745.
McCleary, W.R. 1996. The activation of PhoB by acetylphosphate. *Mol. Microbiol*. **20:** 1155–1163.
McRee, D.E. 1999. XtalView/Xfit—A versatile program for manipulating atomic coordinates and electron density. *J. Struct. Biol*. **125:** 156–165.
Mizuno, T. 1997. Compilation of all genes encoding two-component phosphotransfer signal transducers in the genome of *Escherichia coli*. *DNA Res*. **4:** 161–168.
Murshudov, G.N., Vagin, A.A., and Dodson, E.J. 1997. Refinement of macromolecular structures by the maximum-likelihood method. *Acta Crystallogr. D Biol. Crystallogr*. **53:** 240–255.
Otwinowski, Z. and Minor, W. 1997. Processing of X-ray diffraction data collected in oscillation mode. *Methods Enzymol*. **276:** 307–326.
Polarek, J.W., Williams, G., and Epstein, W. 1992. The products of the *kdpDE* operon are required for expression of the Kdp ATPase of *Escherichia coli*. *J. Bacteriol*. **174:** 2145–2151.
Raivio, T.L. and Silhavy, T.J. 1997. Transduction of envelope stress in *Escherichia coli* by the Cpx two-component system. *J. Bacteriol*. **179:** 7724–7733.
Rhoads, D.B., Laimins, L., and Epstein, W. 1978. Functional organization of the *kdp* genes of *Escherichia coli* K-12. *J. Bacteriol*. **135:** 445–452.
Robinson, V.L., Buckler, D.R., and Stock, A.M. 2000. A tale of two components: A novel kinase and a regulatory switch. *Nat. Struct. Biol*. **7:** 628–633.
Robinson, V.L., Hwang, J., Fox, E., Inouye, M., and Stock, A.M. 2002. Domain arrangement of Der, a switch protein containing two GTPase domains. *Structure (Camb.)* **10:** 1649–1658.
Robinson, V.L., Wu, T., and Stock, A.M. 2003. Structural analysis of the domain interface in DrrB, a response regulator of the OmpR/PhoB subfamily. *J. Bacteriol*. **185:** 4186–4194.
Rossman, M.G. 1990. The molecular replacement method. *Acta Crystallogr. A* **46:** 73–82.
Simon, G., Mejean, V., Jourlin, C., Chippaux, M., and Pascal, M.C. 1994. The *torR* gene of *Escherichia coli* encodes a response regulator protein involved in the expression of the trimethylamine *N*-oxide reductase genes. *J. Bacteriol*. **176:** 5601–5606.
Simon, G., Jourlin, C., Ansaldi, M., Pascal, M.C., Chippaux, M., and Mejean, V. 1995. Binding of the TorR regulator to *cis*-acting direct repeats activates *tor* operon expression. *Mol. Microbiol*. **17:** 971–980.
Stock, A.M., Robinson, V.L., and Goudreau, P.N. 2000. Two-component signal transduction. *Annu. Rev. Biochem*. **69:** 183–215.
Storoni, L.C., McCoy, A.J., and Read, R.J. 2004. Likelihood-enhanced fast rotation functions. *Acta Crystallogr. D Biol. Crystallogr*. **60:** 432–438.
Tabor, S. and Richardson, C.C. 1985. A bacteriophage T7 RNA polymerase/promoter system for controlled exclusive expression of specific genes. *Proc. Natl. Acad. Sci*. **84:** 1074–1078.
Toro-Roman, A., Mack, T.R., and Stock, A.M. 2005. Structural analysis and solution studies of the activated regulatory domain of the response regulator ArcA: A symmetric dimer mediated by the α4-β5-α5 face. *J. Mol. Biol*. **349:** 11–26.
Vaguine, A.A., Richelle, J., and Wodak, S.J. 1999. SFCHECK: A unified set of procedures for evaluating the quality of macromolecular structure-factor data and their agreement with the atomic model. *Acta Crystallogr. D Biol. Crystallogr*. **55:** 191–205.
Volz, K. 1993. Structural conservation in the CheY superfamily. *Biochemistry* **32:** 11741–11753.
Walderhaug, M.O., Polarek, J.W., Voelkner, P., Daniel, J.M., Hesse, J.E., Altendorf, K., and Epstein, W. 1992. KdpD and KdpE, proteins that control expression of the *kdpABC* operon, are members of the two-component sensor-effector class of regulators. *J. Bacteriol*. **174:** 2152–2159.
Wösten, M.M. and Groisman, E.A. 1999. Molecular characterization of the PmrA regulon. *J. Biol. Chem*. **274:** 27185–27190.
Yan, D., Cho, H.S., Hastings, C.A., Igo, M.M., Lee, S.Y., Pelton, J.G., Stewart, V., Wemmer, D.E., and Kustu, S. 1999. Beryllofluoride mimics phosphorylation of NtrC and other bacterial response regulators. *Proc. Natl. Acad. Sci*. **96:** 14789–14794.